Chinese Chemical Letters 35 (2024) 109295

Contents lists available at ScienceDirect

Chinese Chemical Letters

journal homepage: www.elsevier.com/locate/cclet

Photoluminescence and photothermal conversion in boric acid derived carbon dots for targeted microbial theranostics

Yiqiao Chen[a,b], Ao Liu[b], Biwen Yang[b], Zhenzhen Li[b], Binggang Ye[c], Zhouyi Guo[b], Zhiming Liu[b,*], Haolin Chen[a,*]

[a] Department of Anesthesiology, General Hospital of Southern Theater Command of People's Liberation Army, Guangzhou 510010, China
[b] MOE Key Laboratory of Laser Life Science & Guangdong Provincial Key Laboratory of Laser Life Science, College of Biophotonics, South China Normal University, Guangzhou 510631, China
[c] Healthy Medical Engineering Technology Research Center, Guangdong Food and Drug Vocational College, Guangzhou 510520, China

ARTICLE INFO

Article history:
Received 28 September 2023
Revised 7 November 2023
Accepted 9 November 2023
Available online 11 November 2023

Keywords:
Theranostic carbon dots
Fluorescence imaging
Phenylboronic acid
Photothermal therapy
Nanotheranostic

ABSTRACT

Theranostic carbon dots (CDs) have attracted widespread attention recently due to their tunable optical properties and diverse bioactivities. Beyond fluorescent imaging application, the photothermal property endows CDs with the potential for microbial inactivation. However, realization of the effective conversion between fluorescence and heat in one CD system has rarely been reported. Herein, we provide a simple strategy for targeted microbial theranostics based on 4-carboxyphenylboronic acid-derived CDs (PCBA-CDs) which possess concentration-dependent photoluminescence/photothermal features. At lower concentrations, PCBA-CDs show bright and stable fluorescent signals ranging from blue to green. The fluorescence intensity gradually decreases with increasing concentration, while on the contrary, the photothermal effect of PCBA-CDs ascends progressively due to the rearrangement of electronic transitions in aggregated CDs. PCBA-CDs also demonstrate high affinity to the polysaccharide structures on the surface of microbe which allows rapid microbial fluorescence imaging as well as specific photothermal ablation of pathogens in skin wounds using PCBA-CDs at lower and higher concentrations, respectively. This study supplies a facile nanotheranostic strategy for just-in-time microbial management using bioactive CDs.

Pathogenic microbial infection is one of the most serious threats to human health in the world today. The diseases caused by fungi and bacteria exhibit varying degrees of harm to the human body, with severe pathogen infections potentially resulting in fatality [1]. Thus, the prompt detection and timely treatment of hazardous pathogenic microorganisms hold immense significance for both public health and epidemiological research. The diagnosis and treatment of pathogens has been extensively investigated in clinical settings [2]. Methods commonly used for identification of pathogen infection include morphological observation, polymerase chain reaction (PCR) and serological tests, which are often constrained by the expensive equipment, complex training requirements and lengthy detection periods [3–5]. Fluorescence imaging benefiting from its high sensitivity, operability, and convenience has been developed as a non-invasive and efficient technique for real-time monitoring of pathogenic microorganisms [6–8]. On the other hand, the elimination of pathogenic bacteria after visualization contributes to prevent further infection in time, which however is rarely completed using current fluorescent probes. Therefore, it is imperative to amalgamate diagnostic and therapeutic approaches for pathogenic microorganisms in order to enhance the efficacy of rapid eradication in cases of pathogenic microbial infections.

Recently, collaborative strategies that integrate photothermal therapy (PTT) with real-time fluorescence diagnostic methods have been actively pursued owing to the efficient, noninvasive and easy-to-operate properties [9–11]. PTT typically employs near-infrared (NIR) light-absorbing agents that convert laser energy into heat, inducing irreversible cellular damage to pathogenic microorganisms and circumventing drug resistance [12,13]. This renders PTT an optimal choice in conjunction with fluorescence imaging for the theranostic of pathogenic infections. To date, the reported PTT agents have predominantly focused on noble metal nanoparticles and NIR organic dyes such as indocyanine green and IR780 [14,15]. However, these materials exhibit certain limitations, including inadequate thermal stability, potential toxicity associated with heavy metal elements, low absorption coefficients within the red to NIR spectral range, and the possibility of visceral deposition [16–19].

* Corresponding authors.
E-mail addresses: liuzm021@126.com (Z. Liu), chenhlin8@mail2.sysu.edu.cn (H. Chen).

https://doi.org/10.1016/j.cclet.2023.109295
1001-8417/

Carbon dots (CDs), as an emerging type of carbon nanomaterials, have demonstrated their potential in fluorescence imaging and PTT function for the treatment of microorganisms [20–23]. Fluorescent CDs offer distinct advantages in bioimaging and microbial identification due to their excellent biocompatibility, adjustable optical characteristics, and remarkable photostability stability [24–29]. Till date, several groups have reported different fluorescence emissive CDs and them were successfully employed in bioimaging [30–32]. However, the single fluorescence imaging still could not satisfy the urgent demand in accurate treatment of pathogenic microorganisms. In recent years, CDs have emerged as promising candidates for photothermal therapy in various biomedical applications [33,34]. Several approaches have been proposed to modulate the optical and photophysical properties of CDs, including tuning the degree of carbon core conjugation and surface engineering, which achieves red-shift absorption and facilitates efficient photothermal conversion [35–38]. Compared to conventional photothermal nanomaterials, CDs possess several advantages including low toxicity, excellent water solubility, cost-effectiveness, and have demonstrated successful applications in the photothermal treatment of pathogenic microorganisms [39,40]. However, the integration of fluorescence imaging and photothermal therapy poses a significant challenge their inherently opposing optical properties, making it arduous to combine in a single material system. Previous studies on CDs only focused on their fluorescence imaging or PTT application separately, while development of CDs with both fluorescence and PTT capabilities has not been particularly considered [41–45].

In this study, a kind of 4-carboxyphenylboronic acid-derived carbon dots (PCBA-CDs) with microbe-targeted and photoluminescence-photothermal convertible features is supplied for pathogen theranostics. The surface of PCBA-CDs is plentiful of boric acid residues that have been considered as the effective ligands for the polysaccharide structures of microbial cell wall [46]. The photoluminescence (PL) characteristic of PCBA-CDs is concentration-dependent, where the fluorescence emission gradually redshifts from blue, green to yellow with the concentration of PCBA-CDs increases, along with the corresponding fluorescence intensity decreases. We then perceive an elevating photothermal phenomenon during this process, which can be attributed to the aggregation of CDs through hydrogen bonding and electrostatic interaction, resulting in the rearrangement of electronic transitions. In view of this, we provide a strategy for targeted microbial theranostics based on PCBA-CDs using their concentration-regulated photoluminescence/photothermal features. At low concentration, PCBA-CDs can serve as an efficient fluorescent nanoprobe for fast morphological analysis of fungi. At high concentration, PCBA-CDs exhibit excellent photothermal conversion efficiency that achieves an inhibition rate of Gram-positive bacteria up to 99% under 808 nm NIR irradiation. And the targeted PTT based on PCBA-CDs is finally completed on the bacteria-infected skin wound. Therefore, PCBA-CDs support a simple theranostic strategy for rapid detection of microbial infection and subsequent pathogen elimination.

Carbon dots with functional boronic acid groups were prepared by the microwave method using PCBA, citric acid (CA) and urea as precursors (Fig. S1 in Supporting information). As shown in Fig. S2 (Supporting information), the morphology of PCBA-CDs was characterized using transmission electron microscope (TEM), demonstrating that the PCBA-CDs were torispherical and uniformly distributed in solution (Fig. S2a). The high-resolution TEM (HRTEM) image displays a lattice spacing distance of 0.21 nm, which corresponds to typical ⟨100⟩ facet in graphite (Fig. S2b) [47,48]. Fig. S2c shows that the average diameter of PCBA-CDs is 3.9 nm with distribution ranges from 2.5 nm to 5.5 nm, which is in accordance with Gaussian function. The X-ray diffraction (XRD) pattern displays a broad peak centered at 22° (Fig. S2d) corresponding to the typical peak of CDs as previously reported [44]. The surface structure and composition of the PCBA-CDs were then investigated by spectroscopic techniques. The Fourier transform infrared spectroscopy (FT-IR) spectrum of the PCBA-CDs exhibits distinct absorption bands at 1350, 1179 and 1056 cm^{-1}, which can be attributed to B-O stretching vibration, B-O-H bending vibration and C-B stretching vibration, respectively (Fig. S2e) [49,50]. The band located at 1650 cm^{-1} is ascribed to C=C stretching vibrations. The broad absorption bands from 3350 cm^{-1} to 3500 cm^{-1} indicate the presence of amino (-NH_2) and hydroxyl (-OH) functional groups on the surface of PCBA-CDs. The full X-ray photoelectron spectroscopy (XPS) survey scan in Fig. S2f indicates that the PCBA-CDs mainly consist of C 1s, N 1s, O 1s and B 1s. In the high resolution XPS C 1s, four fitting peaks at 283.5, 284.8, 285.9 and 288.2 eV corresponding to the C-B, C–C/C=C, C–N/C–O and C=O, respectively (Fig. S2g) [51]. The O 1s spectrum (Fig. S2h) can be fitted into two peaks, which probably be assigned to C=O (531.7 eV) and graphitic N (533.2 eV), respectively. The two fitting peaks of B 1s XPS at 191.2 and 192.4 eV are attributed to B-C and B-O bonds, which are well in agreement with the FT-IR data (Fig. S2i) [52]. The solutions containing PCBA-CDs were analyzed for zeta potential values using dynamic light scattering (−6.7 mV), in accordance with the previously reported typical potential value of boric acid-modified CDs (Fig. S3 in Supporting information) [53]. These data show the PCBA-CDs are composing of nano-scale graphite-like cores functionalized with boronic acid groups.

Then the photoluminescence properties of the PCBA-CDs were investigated at different concentrations. As shown in Fig. S4 (Supporting information), a concentration-dependent PL behavior of the PCBA-CDs is observed, where the CDs aqueous solution under 365 nm ultraviolet (UV) light displays continuous redshift PL emission from 0.001 mg/mL to 50 mg/mL. The fluorescence emission spectra reveal a redshift in the optimal PL peak from 432 nm to 582 nm as the concentration of PCBA-CDs increases from 0.01 mg/mL to 10 mg/mL, accompanied by a gradual decrease in fluorescence intensity (Fig. 1a). As illustrated in Fig. S5 (Supporting information), the excitation-emission matrices of PCBA-CDs visualizes this transfer process of fluorescence, where three emission centers (blue, green and yellow) are noticed. We can also observe a new center at higher wavelength region gradually emerges as the concentration increases, which may reflect the aggregation phenomenon of PCBA-CDs, resulting in decreased the effective optical band gap (E_g) and PL redshift [54]. We further compared the emission and excitation spectra of PCBA-CDs at varying concentrations. As shown in Fig. S6 (Supporting information), the red shift of the luminescence center and the enhancement of the excitation peak intensity are consistent with the classical phenomenon of J-aggregates, indicating that PCBA-CDs predominantly form J-aggregates at high concentrations conditions [55].

The ultraviolet–visible (UV–vis)-NIR absorption spectra and fluorescence spectra of PCBA-CDs at different concentrations revealed a concentration-dependent energy transfer process from photoluminescence to NIR absorption, as evidenced by the increase in light absorption across the ultraviolet to near-infrared and decrease in fluorescence emission intensity (Figs. 1a and b). These findings have significant implications for the potential application of PCBA-CDs in PTT [56,57]. The photothermal experiments of PCBA-CDs were then carried out, as illustrated in Fig. 1c. A concentration-dependent temperature elevation is observed in the PCBA-CDs solution under 808 nm (1.5 W/cm^2, 5 min) laser irradiation, and the temperature rises to about 45 °C at the concentration of 1 mg/mL, which is enough for a mild hyperthermia PTT. The temperature does not change significantly after five laser on/off cycles, indicating a stable photothermal effect of PCBA-CDs (Fig. S7 in Supporting information). Fig. 1d shows a schematic diagram of concentration-

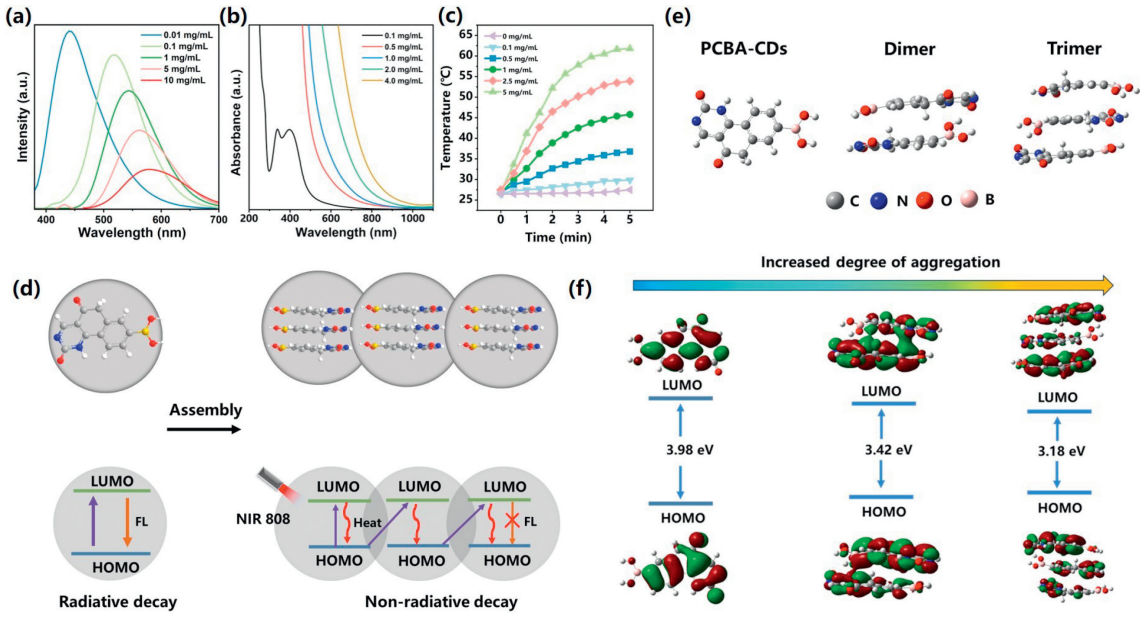

Fig. 1. Concentration-dependent optical features of PCBA-CDs. (a) Fluorescence spectra of PCBA-CDs solutions with concentrations of 0.01, 0.1, 1.0, 5.0 and 10 mg/mL under the excitation of 380 nm. (b) UV–vis-NIR absorption spectra of PCBA-CDs solutions with different concentrations. (c) Temperature elevations of PCBA-CDs aqueous dispersions with different concentrations under 808-nm laser irradiation (1.5 W/cm^2). (d) Scheme of the concentration-induced energy transfer in PCBA-CDs. The red wavy lines symbolize heat generated from the nonradiative decay of electrons at the LUMO level. DFT calculations of PCBA-CDs with increasing aggregation. (e) Molecular structures of the three models and (f) calculated LUMOs and HOMOs of PCBA-CDs, PCBA-CDs dimer, and PCBA-CDs trimer (from left to right).

induced energy transfer process in PCBA-CDs. When the excited electrons of dispersed PCBA-CDs transit back to the highest occupied molecular orbital (HOMO), energy can dissipate through the radioactive decay to generate fluorescence-emission signals. Due to the wide band gap of PCBA-CDs at low concentration, excitation of electrons to lowest unoccupied molecular orbital (LUMO) by NIR laser is not feasible, resulting in a lack of absorption capacity for dispersed PCBA-CDs in the NIR region. However, when the concentration of PCBA-CDs increases, the asymmetric orbital profiles and reduced energy gap promote the respective energy levels of different PCBA-CDs to overlap spatially. Thus, NIR laser can excite electron transitions and energy dissipate through the nonradiative decay to generate heat.

To reveal the concentration-dependent luminescence mechanism of the PCBA-CDs exactly, we simulated three molecular structures using first-principle calculations: PCBA-CDs, the dimer of PCBA-CDs, and the trimer of PCBA-CDs, as shown in Fig. 1e. Geometric optimization, frequency and E_g calculations of the three molecular structures were performed using the hybrid density functional B3LYP with 6–31 G(d, p) basis set in the density functional theory (DFT) calculations [58]. The geometrically optimized as well as the LUMO and HOMO distributions of the three molecular structures are shown in Fig. 1f. The calculated E_g of the molecular structures are 3.98, 3.42, and 3.18 eV, respectively. Based on the above results, a possible formation process of PCBA-CDs producing concentration-dependent fluorescence emission is proposed. Under solvothermal conditions, the dehydration of citric acid and urea produces fluorophore on PCBA [59]. The π-conjugated hexatomic ring bridges the oxygen-associated electron-donating functional groups, forming a donor-π-conjugated acceptor structure in the fluorophore. With the increasing concentration of PCBA-CDs, the PCBA-CDs monomer forms dislocated face-to-face dimers and trimers through hydrophobic interactions and π-π stacking, indicating the gradual formation of J-aggregates [60]. When the concentration further increases, the aggregation degree of PCBA-CDs gradually increases, and the fluorophores between the aggregations begin to form tetramers or even multimers, so the PL wavelength further red-shifts to yellow emission. We transformed the UV–vis-NIR absorption spectra of PCBA-CDs at various concentrations into Tauc curves and subsequently determined the alterations in the E_g. These changes were mutually confirmed with theoretical calculations, as depicted in Fig. S8 (Supporting information), where the E_g values of PCBA-CDs at 0.1, 0.5, 1.0, 2.0, and 4.0 mg/mL were calculated as 2.65, 2.36, 2.16, 1.86, and 1.72 eV, respectively. This result demonstrates that the effective E_g values steadily drop as the concentration increases owing to the quantum confinement effect. Therefore, the data theoretically explain the phenomenon that the emission wavelength of PCBA-CDs can be tuned in the large visible region by simply adjusting the concentration.

Cytotoxicity of PCBA-CDs was measured by cell counting kit-8 (CCK-8) assay before bio-applications. The cell viabilities of 3T3 cells exposed to PCBA-CDs are higher than 85% even at a concentration of up to 5.0 mg/mL (Fig. S9 in Supporting information). Similar result is also verified by the hemolysis test (Fig. S10 in Supporting information), indicating a good biocompatibility of PCBA-CDs.

Microscopic examination is often used for the preliminary detection of pathogenic fungi in clinical practice, and fluorescent reagents can assist clinicians achieving rapid morphological detection of fungi. With this background, the fluorescence imaging ability of PCBA-CDs at low concentrations for fungal morphology was investigated using yeast and filamentous forms, two common fungal forms, as the models. It can be observed from the Fig. 2a that the *Saccharomyces cerevisiae* (*S. cerevisiae*) and *Schizophyllum commune* (*S. commune*) cells are rapidly illuminated by PCBA-CDs through a wash-free staining method, where the morphologies of individual cells can be clearly distinguished. We can also observe that fungal cells emit blue and green fluorescence signals after being stained with 0.01 and 0.1 mg/mL of PCBA-CDs, respectively, confirming the concentration-related fluorescent emission of PCBA-CDs *in vitro*. In comparison, the bioimaging effect of 0.1 mg/mL of PCBA-CDs is better than that of 0.01 mg/mL. For morphological analysis, *S. cerevisiae* cells are spherical and tend to cluster together, while the *S. commune* cells show rare spores,

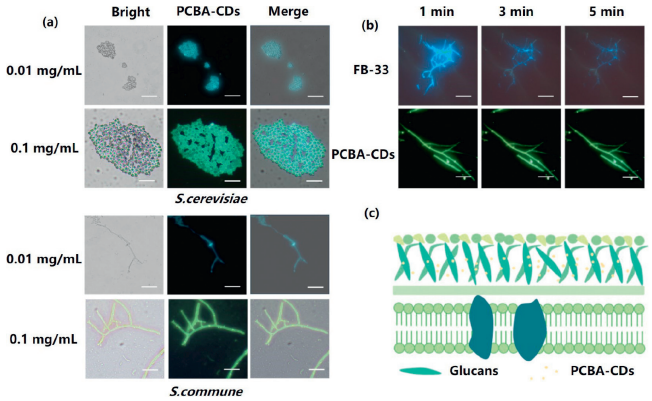

Fig. 2. Rapid microbial morphologic observation using fluorescent PCBA-CDs at lower concentrations. (a) Fluorescence images of *S. cerevisiae* and *S. commune* after staining with PCBA-CDs at 0.01 and 0.1 mg/mL, respectively. (b) The fluorescent stability of PCBA-CDs for *S. commune* imaging, compared to commercial FB-33 dye. (c) Schematic diagram of the targeted mechanism of PCBA-CDs to microbe. Scale bars: 20 μm.

obvious hyphal separation, and typical lock-like association and acicular protrusions. The imaging effect of PCBA-CDs was then compared with that of commercial fluorescein reagent FB-33. As demonstrated in Fig. 2b, the fluorescence images of *S. commune* cells stained with PCBA-CDs are more readable with eye-friendly color and low background. Additionally, the fluorescence signals of PCBA-CDs exhibit enhanced stability compared to FB-33 during a 5-min observation period, thereby establishing them as superior candidates for long-term bioimaging. We speculate that the fast and high-quality fluorescence imaging might be ascribed to the targeting capacity of PCBA-CDs whose functional groups (boric acid residues) display a high affinity to the glucan composition on the surface of fungi (Fig. 2c) [61].

In order to explore the *in vitro* photothermal ability of PCBA-CDs at higher concentrations, photothermal antibacterial tests were performed on Gram-positive and Gram-negative bacteria using PCBA-CDs at 1 mg/mL. Under NIR laser treatment (808 nm, 1.5 W/cm^2), PCBA-CDs exhibit a broad spectrum of antibacterial activity against both types of bacteria (Fig. 3a). For comparison, the antibacterial effect of PCBA-CDs on Gram-positive bacteria such as *Staphylococcus aureus* (*S. aureus*) and *Listeria monocytogenes* (*List*) is more pronounced, which is calculated to be 99% (Fig. S11 in Supporting information), much higher than that on Gram-negative *Escherichia coli* (*E. coli*) and *Pseudomonas aeruginosa* (*P. aeruginosa*) (~80%). Calcein-AM/propidium iodide (PI) live/dead staining assay also confirms the better photothermal antibacterial capacity of PCBA-CDs to Gram-positive bacteria (Fig. 3b). We further speculated the action mechanisms of PCBA-CDs against the two types of bacteria in order to explain the differential antibacterial effect. It has been considered that boric acid can efficiently bind to the peptidoglycan structures on the cell walls of bacteria [62]. However, the peptidoglycan layer of Gram-positive bacteria is much thicker than that of Gram-negative bacteria. Therefore, we consider that more PCBA-CDs are adhered to the surface of Gram-positive bacteria, leading to enhanced antibacterial efficacy under NIR laser exposure (Fig. 3c).

We finally performed the PCBA-CDs-based NIR PTT on bacterial infected skin wounds *in vivo*. All animal procedures were in accordance with Institutional Animal Care and Use Committee (IACUC) guidelines. The methods used in the experiment were approved by the Animal Ethics Committee of South China Normal University. After NIR laser irradiation, the temperature of the skin wound treated with PCBA-CDs (1 mg/mL) rises to 45 °C (Fig. 4a), indicating a mild hyperthermia for photothermal treatment of infected skin wound. Fig. 4b exhibits the photographs of the infected skin wounds after NIR PTT during a 10-day observation, where gradually healing wound tissues in all groups are noticed. On day 10, only 10.17% of the wound area remains in PCBA-CDs+NIR group,

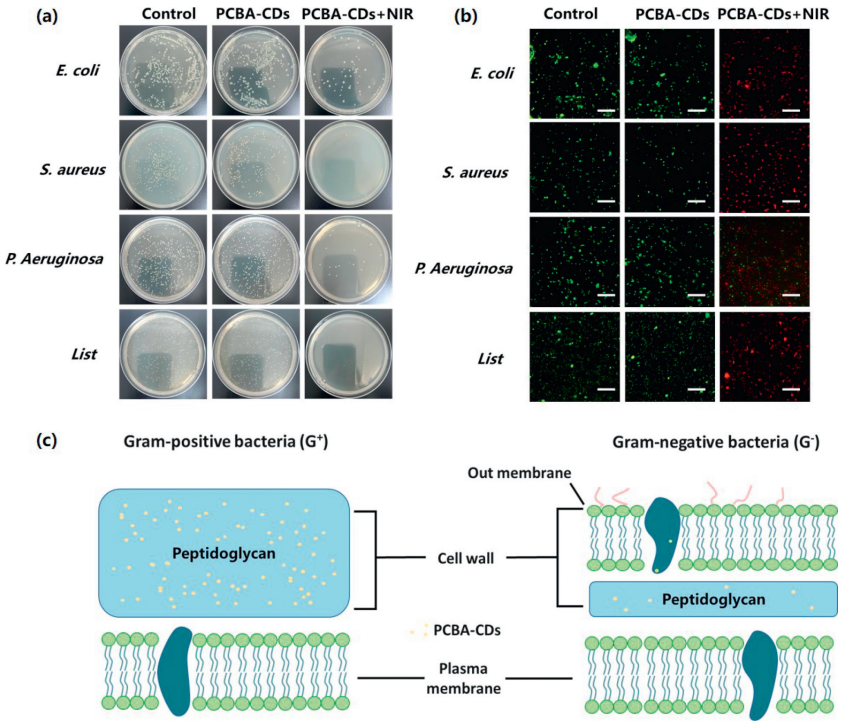

Fig. 3. Photothermal antibacterial effect of PCBA-CDs *in vitro*. (a) Agar plate digital photographs of bacterial colonies after PCBA-CDs mediated NIR PTT. (b) The corresponding calcein-AM/PI images of bacteria (scale bar: 20 μm). (c) Schematic diagram shows the differential antibacterial effect of PCBA-CDs to Gram-positive and Gram-negative bacteria.

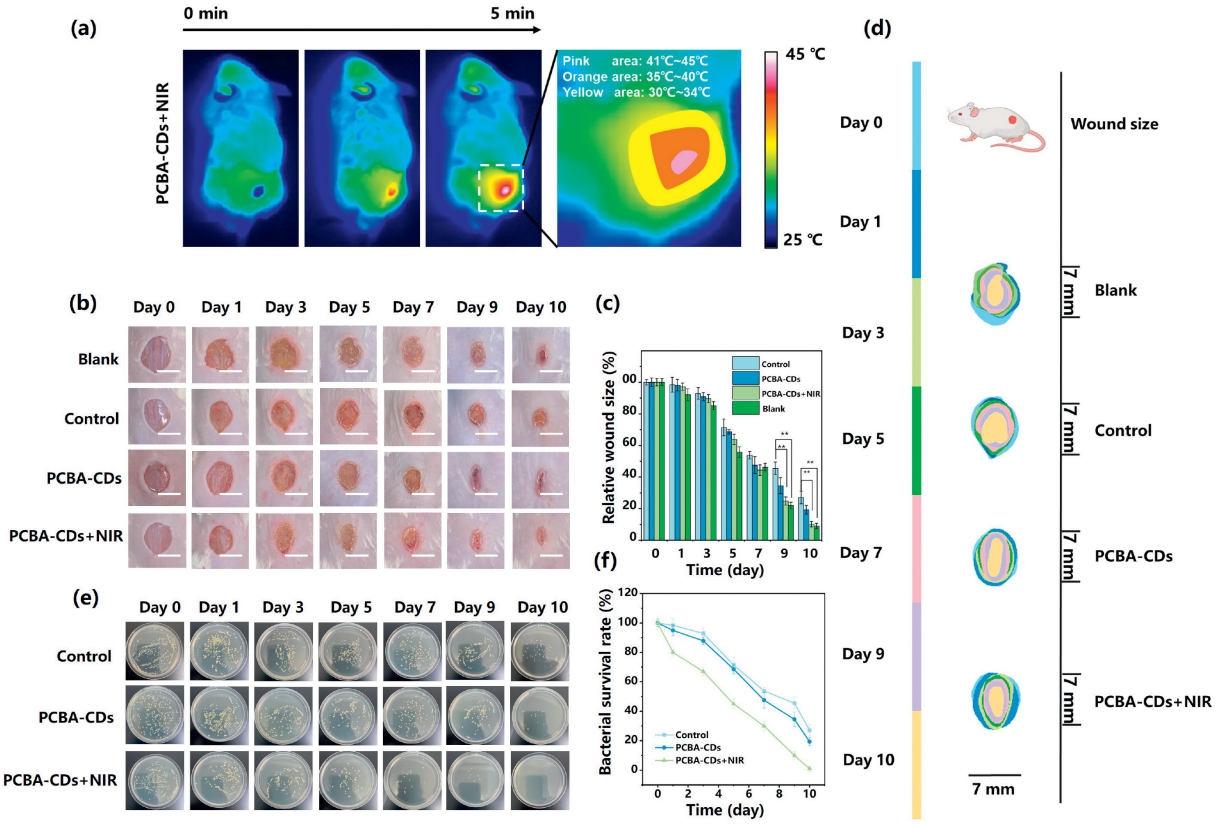

Fig. 4. (a) Thermal images variations of mice treated with PCBA-CDs after NIR irradiation for 5 min (1.5 W/cm^2, 808 nm). (b) Photographs of the *S. aureus* infected skin wounds on BALB/c mice during 10 days of observation (scale bar: 5 mm) statistical analysis of (c) corresponding relative wound sizes. (d) Relevant alterations in wound size over the course of time. (e) Photographs and (f) quantitative analysis of bacterial colonies from tissues of different treatment groups (n=3, $^{**}P < 0.01$).

compared to 27.08% in control group (Fig. 4c), indicating that NIR-induced mild hyperthermia based on PCBA-CDs can enhance the bacterial killing efficacy. The images of wounds at different time intervals were then overlapped using Image J software. Compared with control (infected wound without treatment) group, the wound healing speed in PCBA-CDs+NIR group is significantly faster (Fig. 4d). To further quantitatively evaluate the anti-infective performance of PCBA-CDs-based PTT, the bacteria around the wounds were cultured and counted after treatment. The PCBA-CDs+NIR group presents the lowest number of bacterial colonies compared with other infected groups (Figs. 4e and f). These results coincide well with the data about skin wound size.

The wounds of skin were collected at the end of treatment and evaluated by hematoxylin and eosin (H&E) staining. As shown in Fig. S12 (Supporting information), the number of neutrophils decreases significantly and newly formed vessels occur in the PCBA-CDs+NIR group, which is similar to that of blank (uninfected skin wound) group, while the inflammatory reaction is still severe in the control and PCBA-CDs groups. Scanning electron microscopy (SEM) was finally carried out to observe the morphologies of bacterial cells after interaction with PCBA-CDs. As shown in Fig. S13 (Supporting information), *S. aureus* cells without any treatment (control group) remain intact membrane. When *S. aureus* cells are treated with PCBA-CDs (1.0 mg/mL) in the absence of NIR irradiation, partial agglutination is observed on the cellular surface, which may be due to the binding of PCBA-CDs to the cell wall, but the morphology of the bacteria is not affected indicating that the cells are almost viable. After treatment with PCBA-CDs+NIR, sunken and collapsed *S. aureus* cells with wrinkled membranes are distinctly noted, confirming the excellent photothermal inactivation of bacteria based on PCBA-CDs.

Biotoxicity is considered as a significant factor in the development of antibacterial nanomaterials. The body weight of the mice shows no noticeable weight loss after undergoing PCBA-CDs-based NIR PTT (Fig. S14 in Supporting information). Blood biochemical and histological analyses were also conducted to evaluate the biocompatibility of the as-prepared PCBA-CDs *in vivo* (Fig. S15 in Supporting information). The parameters of white blood cells (WBC), red blood cells (RBC), hemoglobin (HGB), hematocrit (HCT), mean corpuscular volume (MCV) and mean corpuscular hemoglobin concentration (MCHC) in whole blood were selected to evaluate the cytotoxicity of the PCBA-CDs by hematology assessment. The data reveal that all the indicators are normal in the treatment group compared with control group. The major organs like heart, liver, spleen, lung and kidney were also collected for H&E staining. No physiological lesions are observed (Fig. S16 in Supporting information), which further confirms the *in vivo* safety of PCBA-CDs.

In conclusion, a type of CDs with boric acid group was developed by microwave method (PCBA-CDs). The optical properties of PCBA-CDs are tunable *via* simply adjusting of their concentration. PCBA-CDs can emit bright green fluorescence signals at low concentrations (0.1 mg/mL) while displaying promising NIR photothermal features at high concentrations (1 mg/mL), which may be attributed to the energy transfer process caused by the aggregation of CDs resulting in the rearrangement of electronic transitions in PCBA-CDs. This concentration-dependent photoluminescence/photothermal feature enables PCBA-CDs as novel nanoprobe for microbial theranostics. In addition, the boric acid residues on PCBA-CDs also show high affinity to the polysaccharide structure on microbial cell walls. Therefore, fast and wash-free morphological fluorescence detection of microbes, as well as targeted NIR PTT of infected skin wounds have been successfully achieved

using PCBA-CDs at different concentrations. This strategy based on PCBA-CDs with tunable optical properties is expected to bring new approaches to the diagnosis and treatment of microorganisms.

Declaration of competing interest

The authors declare that they have no known competing financial interests or personal relationships that could have appeared to influence the work reported in this paper.

Acknowledgments

This work was supported by the National Natural Science Foundation of China (Nos. 32071399 and 62175071), the Guangdong Basic and Applied Basic Research Foundation (Nos. 2021A1515011988 and 2021A1515110265), the Science and Technology Program of Guangzhou (No. 2019050001), the Project on the Education Department of Guangdong (Nos. 2021KTSCX238 and 2022ZDZX2077), and the Natural Science Research Project of Guangdong Food and Drug Vocational College (Nos. 2020ZR01 and 2022ZR02).

Supplementary materials

Supplementary material associated with this article can be found, in the online version, at doi:10.1016/j.cclet.2023.109295.

References

[1] D.F. Niño, C.P. Sodhi, D.J. Hackam, Nat. Rev. Gastroenterol. Hepatol. 13 (2016) 590–600.
[2] G. Xing, W. Zhang, N. Li, et al., Chin. Chem. Lett. 33 (2022) 1743–1751.
[3] S.B. Somvanshi, A.M. Ulloa, M. Zhao, et al., Biosens. Bioelectron. 207 (2022) 114214.
[4] C.S. Ho, N. Jean, C.A. Hogan, et al., Nat. Commun. 10 (2019) 4927.
[5] A. Liu, Y. Chen, B. Yang, et al., Nanophotonics 11 (2022) 5121–5131.
[6] Q. Ma, X. Sun, W. Wang, et al., Chin. Chem. Lett. 33 (2022) 1681–1692.
[7] W. Li, G.S.K. Schierle, B.F. Lei, et al., Chem. Rev. 122 (2022) 12495–12543.
[8] X. Shen, W. Xu, J. Ouyang, et al., Chin. Chem. Lett. 33 (2022) 4505–4516.
[9] R.M. Jiang, J. Dai, X.Q. Dong, et al., Adv. Mater. 33 (2021) 2101158.
[10] Y.Q. Yang, X.X. Fan, L. Li, et al., ACS Nano 14 (2020) 2509–2521.
[11] Y. Qin, X.H. Chen, Y.X. Gui, et al., J. Am. Chem. Soc. 144 (2022) 12825–12833.
[12] Y. Liu, P. Bhattarai, Z. Dai, et al., Chem. Soc. Rev. 48 (2019) 2053–2108.
[13] H.S. Jung, P. Verwilst, A. Sharma, et al., Chem. Soc. Rev. 47 (2018) 2280–2297.
[14] H. Xu, Q. Li, L. Wang, et al., Chem. Soc. Rev. 43 (2014) 2650–2661.
[15] N. Li, P. Zhao, D. Astruc, Angew. Chem. Int. Ed. 53 (2014) 1756–1789.
[16] W.H. Chen, G.F. Luo, Q. Lei, et al., ACS Nano 11 (2017) 1419–1431.
[17] C. You, Y. Li, Y. Dong, et al., ACS Biomater. Sci. Eng. 6 (2020) 1535–1542.
[18] X. Lin, Y. Fang, Z. Hao, et al., Small 17 (2021) e2103303.
[19] F. Lin, C. Jia, F.G. Wu, Small Struct. 3 (2022) 2200033.
[20] Q. Zhang, R. Wang, B. Feng, et al., Nat. Commun. 12 (2021) 6859.
[21] Y. Bai, J. Zhao, S. Wang, et al., ACS Appl. Mater. Interfaces 13 (2021) 35365–35375.
[22] M.L. Bhaisare, G. Gedda, M.S. Khan, et al., Anal. Chim. Acta 920 (2016) 63–71.
[23] S. Huang, Y. Song, J.R. Zhang, et al., Small 19 (2023) 2207385.
[24] S.H. Miao, K. Liang, J.J. Zhu, et al., Nano Today 33 (2020) 100879.
[25] S. Majumdar, G. Krishnatreya, N. Gogoi, et al., ACS Appl. Mater. Interfaces 8 (2016) 34179–34184.
[26] L.M. Zhai, Y. Zhao, R.L. Xiao, et al., Nanoscale 14 (2022) 14645–14660.
[27] X. Zhao, J. Yang, J. Zhang, et al., Eur. J. Pharm. Biopharm. 174 (2022) 47–55.
[28] T. Garcia-Millan, T.A. Swift, D.J. Morgan, et al., Nanoscale 14 (2022) 6930–6940.
[29] J. Yue, P. Miao, L. Li, et al., ACS Appl. Mater. Interfaces 14 (2022) 49582–49591.
[30] Y. Ma, Z. Ma, X. Huo, et al., J. Agric. Food Chem. 68 (2020) 10223–10231.
[31] X.W. Yu, X. Liu, Y.W. Jiang, et al., Anal. Chem. 94 (2022) 4243–4251.
[32] L. Tong, X. Wang, Z. Chen, et al., Anal. Chem. 92 (2020) 6430–6436.
[33] M. Fang, B. Wang, X. Qu, et al., Chin. Chem. Lett. 35 (2024) 108423.
[34] B. Wang, H. Cai, G.I.N. Waterhouse, et al., Small Sci. 2 (2022) 2200012.
[35] H. Yan, H. Ni, Y. Yang, et al., Chin. Chem. Lett. 31 (2020) 1792–1796.
[36] Y. Zhang, H. Xia, M. Yang, et al., Chin. Chem. Lett. 34 (2023) 108197.
[37] E. Liu, J. Wu, T. Liang, et al., Chin. J. Chem. 41 (2023) 1994–2001.
[38] X. Yang, X. Li, B. Wang, et al., Chin. Chem. Lett. 33 (2022) 613–625.
[39] Y. Yan, J. Gong, J. Chen, et al., Adv Mater. 31 (2019) e1808283.
[40] Y.J. Chung, J. Kim, C.B. Park, ACS Nano 14 (2020) 6470–6497.
[41] D. Li, D. Han, S.N. Qu, et al., Light Sci. Appl. 5 (2016) e16120.
[42] J. Liu, Y. Geng, D. Li, et al., Adv. Mater. 32 (2020) e1906641.
[43] H. Zhang, G. Wang, Z. Zhang, et al., Light Sci. Appl. 11 (2022) 113.
[44] Y. Zhang, K. Liu, J. Yu, et al., Nano Res. 15 (2021) 6399–6406.
[45] S.J. Wang, Y.Q. Zhang, P. Zhuo, et al., J. Mater. Chem. B 8 (2020) 5877–5882.
[46] Y.Y. Aung, A.N. Kristanti, H.V. Lee, et al., ACS Omega 6 (2021) 17750–17765.
[47] H. Yang, Y. Liu, Z. Guo, et al., Nat. Commun. 10 (2019) 1789.
[48] Y. Ru, L. Sui, H. Song, et al., Angew. Chem. Int. Ed. 60 (2021) 14091–14099.
[49] P. Shen, Y. Xia, Anal. Chem. 86 (2014) 5323–5329.
[50] X.L. Sun, B.M. Chapin, P. Metola, et al., Nat. Chem. 11 (2019) 768–778.
[51] L. Jiang, H. Ding, S. Lu, et al., Angew. Chem. Int. Ed. 59 (2020) 9986–9991.
[52] S. Cui, B. Wang, Y. Zan, et al., Chem. Eng. J. 431 (2022) 133373.
[53] M.S. Wu, Z.R. Zhou, X.Y. Wang, et al., Anal. Chem. 94 (2022) 2882–2890.
[54] C.T. Chien, S.S. Li, W.J. Lai, et al., Angew. Chem. Int. Ed. 51 (2012) 6662–6666.
[55] D. Qu, D. Yang, Y. Sun, et al., J. Phys. Chem. Lett. 10 (2019) 3849–3857.
[56] D. Xi, M. Xiao, J. Cao, et al., Adv. Mater. 32 (2020) 1907855.
[57] Y. Liu, W. Zhen, L. Jin, et al., ACS Nano 12 (2018) 4886–4893.
[58] Y. Liu, J.H. Lei, G. Wang, et al., Adv. Sci. 9 (2022) 2202283.
[59] L. Shi, J.H. Yang, H.B. Zeng, et al., Nanoscale 8 (2016) 14374–14378.
[60] Z. Man, Z. Lv, Z. Xu, et al., Adv. Funct. Mater. 30 (2020) 2000105.
[61] B. Tian, T. Fu, Y. Wan, et al., J. Nanobiotechnol. 19 (2021) 456.
[62] R. Li, J. Yan, B. Feng, et al., ACS Appl. Mater. Interfaces 15 (2023) 18663–18671.